Gas-Phase Oligomerization of Propene Initiated by Benzene Radical Cation

Yezdi B. Pithawalla, Michael Meot-Ner, Junling Gao, and M. Samy El Shall*

Department of Chemistry, Virginia Commonwealth University, Richmond, Virginia 23284-2006

Vladimir I. Baranov and Diethard K. Bohme

Department of Chemistry, York University, Toronto, Ontario, Canada

Received: September 21, 2000; In Final Form: December 18, 2000

Initiation of the radical cation polymerization of propene has been observed following the selective ionization of benzene in the gas phase by resonance two-photon ionization−high-pressure mass spectrometry (R2PI−HPMS) and by selected ion flow tube (SIFT) techniques. In this system, the aromatic initiator (C_6H_6) has an ionization potential (IP) between those of the reactant's monomer (C_3H_6) and its covalent dimer (C_6H_{12}), i.e, IP(C_3H_6) > IP(C_6H_6) > IP(C_6H_{12}). Therefore, direct charge transfer from $C_6H_6^{\bullet+}$ to C_3H_6 is not observed due to the large endothermicity of 0.48 eV, and only the adduct $C_6H_6^{\bullet+}(C_3H_6)$ is formed. However, coupled reactions of charge transfer with covalent condensation are observed according to the overall process $C_6H_6^{\bullet+} + 2C_3H_6 \rightarrow C_6H_{12}^{\bullet+} + C_6H_6$, which results in the formation of a hexene product ion, $C_6H_{12}^{\bullet+}$. The formation of this ion can make the overall process of charge transfer and covalent condensation significantly exothermic. At higher concentrations of propene, the reaction products are the propene oligomers $(C_3H_6)_n^{\bullet+}$ with $n = 2-7$ and the adduct series $C_6H_6^{\bullet+}(C_3H_6)_n$ with $n \leq 6$. The significance of the coupled reactions is that the overall process leads exclusively to the formation of the condensation product $(C_3H_6)_n^{\bullet+}$ and avoids other competitive channels in the ion/molecule reactions of propene. Gas-phase nominal second-order rate coefficients for the overall reaction into both channels are in the range of $(1-3) \times 10^{-12}$ cm^3 s^{-1}. The rate coefficients into both channels, especially for the formation of the $C_6H_{12}^{\bullet+}$ dimer, have large negative temperature dependencies. Consistent with the gas-phase results, the intracluster reactions of $C_6H_6^{\bullet+}$ produced selectively by R2PI of mixed benzene/propene clusters also do not form the monomer ion $C_3H_6^{\bullet+}$ but form higher propene clusters $(C_3H_6)_n^{\bullet+}$ that contain at least the $C_6H_{12}^{\bullet+}$ hexene ion. The similarity of the reaction mechanisms in the gas phase and in preformed clusters suggests that the mechanism may also apply in the condensed phase in common aromatic solvents such as benzene and toluene.

I. Introduction

The study of gas-phase polymerization is an important area of research from both fundamental and practical points of view.[1] Detailed understanding of the early stages of polymerization, exploring new initiation methods, and investigating different termination mechanisms and the role of the solvent in chain transfer and termination reactions are among the possible contributions of gas-phase polymerization to basic polymer science. From a practical point of view, gas-phase polymerization can lead to the synthesis of defect-free, uniform thin polymeric films of controlled morphology and tailored compositions with excellent electrical and optical properties for many technological applications such as protective coatings and electrical insulators.[2−6] Furthermore, gas-phase polymerization eliminates the need for distillation, drying, and solvent recovery and, therefore, the operating costs and the environmental problems associated with these processes. Thus, it is not surprising that the interest in studying gas-phase and cluster polymerization has increased significantly over the past decade.[7−42]

Gas-phase polymerization can be initiated by ionizing radiation, pulse radiolysis, metal cations and dications, and organometallic initiators.[7−42] Charge-transfer (or electron-transfer) reactions represent other initiation mechanisms, where radical cations or anions are capable of starting the propagation process. In the gas phase, charge-transfer reactions usually proceed efficiently when exothermic (or exergonic), and are slow or unobservable when significantly endothermic (or endergonic). However, we observed recently a novel subclass of these reactions in a system of an ionized aromatic (toluene, C_6H_5-$CH_3^{\bullet+}$) and a neutral olefin (isobutene, *i*-C_4H_8) that has a higher ionization potential (IP) than the aromatic molecule.[30,38] In this case charge transfer to a single olefin molecule would be endothermic by 0.42 eV. With an energy barrier at least as large, the rate coefficient would be $k \leq k_{\text{collision}} \exp(-\Delta H°/RT) \approx 10^{-17}$ cm^3 s^{-1}, and the reaction would be unobservable. Indeed, in the reaction system of $C_6H_5CH_3^{\bullet+}$ and *i*-C_4H_8, the formation of *i*-$C_4H_8^{\bullet+}$ was not observed. However, at sufficiently high partial pressures of *i*-C_4H_8, we observed an overall process yielding the covalent dimer ion $C_8H_{16}^{\bullet+}$ according to reaction 1.

$$C_6H_5CH_3^{\bullet+} + 2(i\text{-}C_4H_8) \rightarrow C_8H_{16}^{\bullet+} + C_6H_5CH_3 \quad (1)$$

The overall reaction consisting of charge transfer and covalent bond formation is exothermic by 17.5 kcal/mol and was observed to proceed faster by a factor of 10^5 than predicted for the simple endothermic charge-transfer reaction.[38] Pressure and concentration effects suggested that the reaction proceeds through a reactive intermediate π complex, $(C_6H_5CH_3^{\bullet+})i$-C_4H_8.

10.1021/jp003421b CCC: $20.00
Published on Web 03/23/2001

The partial positive charge transferred to the olefin in the complex activates it for nucleophilic attack by a second olefin molecule, leading to covalent condensation.

It is desirable to extend these studies to other systems to confirm and generalize the new mechanism. Of particular interest is the application of these reactions in developing novel initiation methods for the gas-phase polymerization of olefin monomers.[7−42] For these purposes, we shall investigate the reaction analogous to reaction 1 in an even more simple system of reactants, i.e., reaction 2.

$$C_6H_6^{\bullet+} + 2C_3H_6 \rightarrow C_6H_{12}^{\bullet+} + C_6H_6 \qquad (2)$$

This reaction represents an initiation mechanism for the gas-phase polymerization of propene since it results in the formation of the dimer radical cation, which can sequentially add several propene molecules. In this case, the IP of the aromatic initiator benzene (9.25 eV) is significantly lower than that of the propene molecule (9.73 eV), and thus direct charge transfer from $C_6H_6^{\bullet+}$ to propene is even more endothermic than in the toluene radical cation/isobutene system.[43] The significance of this process is that it leads exclusively to the formation of condensation products $(C_3H_6)_n^{\bullet+}$ and avoids other competitive channels in the ion/molecule reactions of propene. For example, the reactions of $C_3H_6^{\bullet+}$ with neutral C_3H_6 involve several channels starting with the formation of the $C_3H_7^+$, $C_4H_7^+$, and $C_4H_8^{\bullet+}$ ions and their association products. Although several groups have investigated the ion/molecule reactions of propene,[44−59] the formation of higher order condensation products $(C_3H_6)_n^{\bullet+}$ with $n > 2$ in the gas phase has not been reported. Interestingly, intracluster polymerization leading to covalently bonded molecular ions has been proposed to explain the ion distribution resulting from the electron impact ionization of propene clusters.[13,37] In the present paper, we provide evidence for the formation of higher order propene ions $(C_3H_6)_7^{\bullet+}$ by sequential gas-phase polymerization of propene following the generation of the propene dimer cation $(C_3H_6)_2^{\bullet+}$.

To establish the mechanistic features of the initiation process, selective ionization of the aromatic component is necessary to avoid direct ionization of the olefin monomer. For this reason, we use resonant two-photon ionization coupled with high-pressure mass spectrometry (R2PI−HPMS),[60] where the mode of ionization is selective for the aromatic component. Furthermore, to eliminate any problems that could arise from the presence of the neutral aromatic, it is desirable to demonstrate the reaction unequivocally by a tandem method where the ion is generated separately and then injected into a mixture containing only the olefin without the neutral aromatic. This would avoid possible kinetic and mechanistic complications due to the formation of the aromatic dimer cations. For these reasons, we employ the selective ion flow tube (SIFT) technique to study the same reaction.[61] The observation of the initiation process by two independent gas-phase techniques and also in clusters provides further support for the proposed mechanism and establishes a solid ground to investigate analogous systems in the condensed phase.

II. Experimental Section

The mass spectrometric studies were performed using the R2PI−HPMS apparatus that was developed recently.[38,60] Briefly, the HPMS ion source is a cubic aluminum block with a volume of about 2 cm^3, fitted with quartz windows through which the laser beam enters and exits. Gas mixtures are prepared in a 2 L glass flask heated to >100 °C and admitted to the ion source at selected pressures via an adjustable needle valve. The ion source pressure is monitored with a 0.01−10 Torr capacitance manometer coupled with the gas inlet tube. The laser beam is slightly focused within the center of the cell using a quartz spherical lens ($f = 60$ cm, $d = 2.54$ cm). The laser output at $\lambda = 258.9$ nm, 100−300 μJ, $\Delta t = 15$ ns, and a 15 Hz repetition rate is generated by a XeCl excimer-pumped dye laser (Lambda Physik LPX 101 and FL-3002). Coumarin 503 (Exciton) dye laser output passes through a β-BaB_2O_4 crystal (CSK) cut at 52° to generate continuously tunable frequency-doubled output of 10^{-8} s pulses. The spatially filtered ultraviolet radiation passes through the high-pressure cell, and the focusing is adjusted to minimize three-photon processes (i.e., unimolecular fragmentation) and still provides sufficient ion current (photon power density $\sim 10^5$ W/cm^2). The reactant and product ions escape through a precision pinhole (200 μm, Melles Griot) and are analyzed with a quadrupole mass filter. The quadrupole mass filter (Extrel C-50, equipped with 3/8 in. diameter rods and with a resolution better than 1 amu, fwhm) is mounted coaxially onto the ion exit hole. The distance from the ion exit hole to the C50 lens stack is 2 cm. The ion current from the electron multiplier is amplified and recorded with a 350 MHz digital oscilloscope (LeCroy 9450).

The SIFT experiments used the apparatus and methods described previously.[61,62] The measurements were performed at 294 ± 3 K at a helium buffer gas pressure of 0.3 ± 0.01 Torr. The flow zone had an effective reaction length of 71.1 cm. The mean bulk gas velocity was 4783 cm s^{-1}.

Benzene/propene binary clusters were generated by pulsed adiabatic expansion in a supersonic cluster beam apparatus.[10,11,28,30] The essential elements of the apparatus are jet and beam chambers coupled to a time-of-flight (TOF) mass spectrometer. During operation, a vapor mixture of 2−4% benzene and 5−10% propene (Aldrich, 99.9% purity) in He (ultrahigh purity, Spectra Gases, 99.99%) at a pressure of 2−4 atm is expanded through a conical nozzle (500 μm diameter) in pulses of 200−300 μs duration at repetition rates of 6−10 Hz. The jet is skimmed and passed into a high-vacuum chamber, which is maintained at 8×10^{-8} to 2×10^{-7} Torr. The collimated cluster beam passes into the ionization region of the TOF mass spectrometer, where it intersects a laser pulse from a frequency-doubled dye laser. Our TOF mass spectrometer is based on the Wiley−McLaren three-grid space-focusing design.[63] The cluster ions are electrostatically accelerated in a two-stage acceleration region (300−400 V/cm), travel a field-free region (~110 cm in length), and are then accelerated to a two-stage microchannel-plate detector. The TOF spectrum is recorded by digitizing the amplified current output of the detector by a 350 MHz digitizer (LeCroy 9450) and averaged over 500−1000 pulses.

III. Results and Discussion

1. Ion Chemistry of Propene. The ion/molecule chemistry of propene has been studied extensively by ICR,[51,56,57] in a tandem mass spectrometer,[48,50] and by photoionization−HPMS.[52,58] At low pressures the reaction of $C_3H_6^{\bullet+}$ with C_3H_6 yielded $C_4H_8^{\bullet+}$ (43%), $C_3H_7^+$ (24%), $C_5H_9^+$ (20%), and $C_4H_7^+$ (13%) with an overall rate coefficient of 7.4×10^{-10} cm^3 s^{-1}.[48,49,55,57] At higher pressures (0.25 Torr), the dimer cation was observed, although not at a very significant yield.[49] The covalent nature of the dimer has been suggested on the basis of the proposed structures by Futurell[49] ($CH_3CH_2C\dot{H}CH^+CH_2CH_3$) and Peers,[50] who proposed a distonic-type structure (CH_3-$C\dot{H}CH_2CH_2CH^+CH_3$). Concerning the reactivity of the dimer,

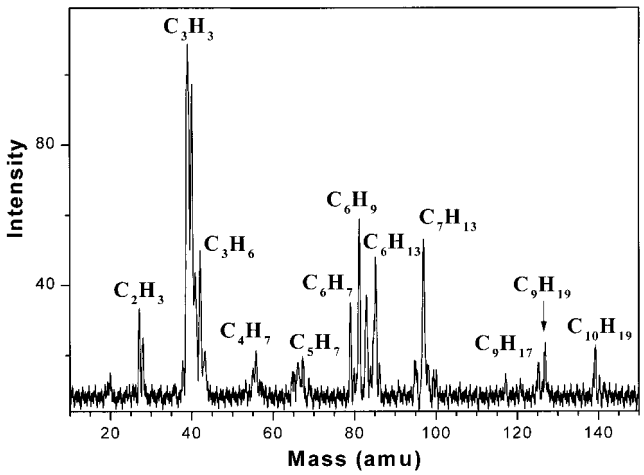

Figure 1. Mass spectrum of 10% propene in Ar obtained with MPI at 248 nm at a source pressure of 0.247 Torr ($N = 7.9 \times 10^{15}$ cm^{-3}).

it has been suggested that the H_2-transfer reaction between $C_6H_{12}^{\bullet+}$ and C_3H_6 (producing $C_6H_{10}^{\bullet+}$ and C_3H_8) occurs only when $C_6H_{12}^{\bullet+}$ has a cyclic structure.[52] When $C_6H_{12}^{\bullet+}$ has an olefinic structure, a condensation process occurs to produce $C_9H_{18}^{\bullet+}$, and higher order products may be expected.[52] However, these species were not observed in previous studies since the reactions were examined mostly under low-pressure conditions.

Before examining the benzene/propene system, we investigated the ion chemistry of propene in Ar carrier gas under the HPMS conditions. The mixture was ionized by nonresonant multiphoton ionization (MPI) using a KrF excimer laser at 248 nm, which resulted in generating Ar^+, Ar^{2+}, $C_3H_6^{\bullet+}$, and other fragment ions. Figure 1 displays the mass spectrum observed following the MPI of 10% propene in Ar at a source pressure of 0.25 Torr, and Figure 2 displays the time profiles of the resulting ions. The major products observed can be classified into four groups as shown in parts a−d of Figure 2. The first group includes the $C_4H_7^+$ (*m*/*z* 55) ion and its adducts with further propene molecules $C_7H_{13}^+$ (*m*/*z* 97) and $C_{10}H_{19}^+$ (*m*/*z* 139). The second group contains the $C_3H_3^+$ and $C_3H_5^+$ ions and their adducts with propene ($C_6H_9^+$ and $C_6H_{11}^+$ respectively). The third and fourth groups include the molecular ion $C_3H_6^{\bullet+}$ and its proton-transfer product to propene ($C_3H_7^+$), along with their higher adducts with propene. The product ions $C_3H_7^+$, $C_4H_7^+$, and $C_5H_9^+$ can also be produced from the bimolecular $C_3H_6^{\bullet+}/C_3H_6$ reactions (3), which were observed by Futrell et al.[48,49]

$$C_3H_6^{\bullet+} + C_3H_6 \longrightarrow [C_6H_{12}^{\bullet+}]^* \longrightarrow \begin{cases} C_3H_7^+ + C_3H_5^\bullet \\ C_4H_7^+ + C_2H_5^\bullet \\ C_5H_9^+ + CH_3^\bullet \end{cases} \quad (3)$$

In addition to the products shown in Figure 2, at higher concentrations of propene, further reactions with propene could lead to larger ions such as $C_3H_7(C_3H_6)_n^+$ ($n \leq 3$) and C_4H_7-$(C_3H_6)_n^+$ ($n \leq 2$). Figure 3 displays the normalized ion intensities of the major ion sequences observed following the MPI of a propene/Ar mixture obtained under the same experimental conditions as the data shown in Figure 2. It is clear that the observed total ion yield of the propene condensation channel $(C_3H_6)_n^{\bullet+}$ is very low [~6% for $(C_3H_6)_2^{\bullet+}$ and 2% for $(C_3H_6)_3^{\bullet+}$]. This result is also consistent with the previous studies of the ion/molecule reactions of propene.[48,49]

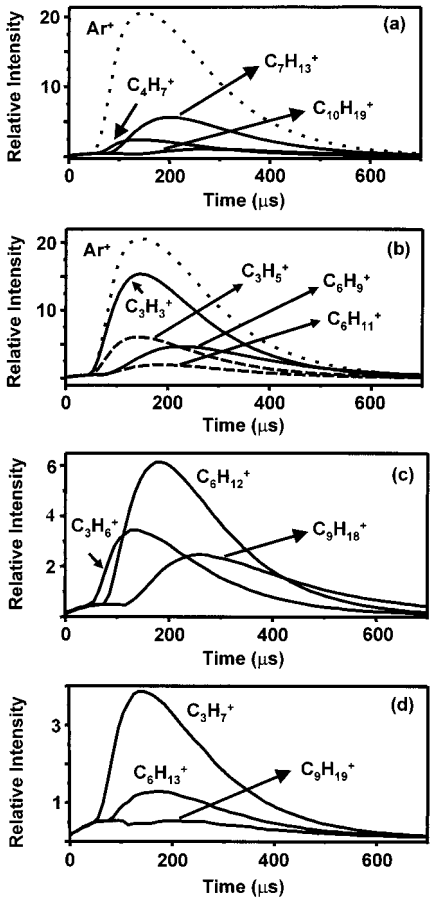

Figure 2. Time profiles of the major ions produced in the propene system, in the absence of benzene, with $P(C_3H_6) = 0.123$ Torr ($N = 3.9 \times 10^{15}$ cm^{-3}) and $P(Ar) = 0.877$ Torr ($N = 2.8 \times 10^{16}$ cm^{-3}) at 298 K.

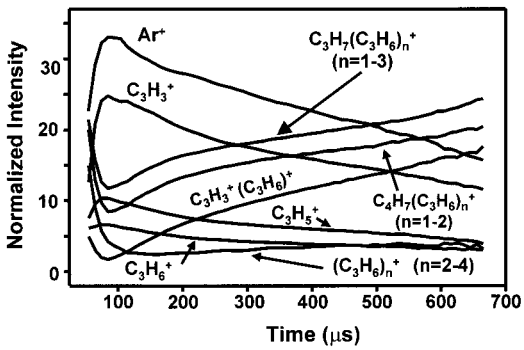

Figure 3. Normalized time profiles of the major ions produced in the propene system following MPI at 248 nm in a mixture of 12.3% propene in Ar at a source pressure of 1 Torr and $T = 298$ K.

The data shown in Figures 1−3 indicate that the primary ions formed by the MPI of the propene/Ar mixture are similar to those previously observed by electron impact (EI)-ICR[51,56,57] and photoionization−HPMS.[52,58] However, under the high-pressure conditions employed in our experiments (1−2 Torr), the formation of higher adducts of the primary ions is significantly enhanced, which leads to complicated sequences of product ions.

2. Benzene/Propene System Ionized by MPI at 248 nm. We extended the HPMS experiments of propene by using a similar mixture but also adding benzene to the reaction mixture, while still ionizing the Ar carrier gas. In this case, Ar^+ and some $C_3H_6^{\bullet+}$ are generated initially, but transfer the charge rapidly to generate $C_6H_6^{\bullet+}$, which becomes the initiator of the

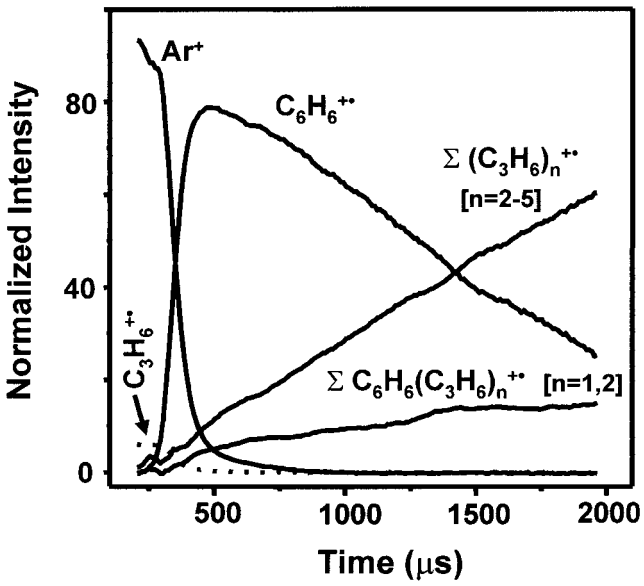

Figure 4. Normalized time profiles with $P(C_6H_6) = 0.000\,068$ Torr ($N = 2.19 \times 10^{12}$ cm^{-3}), $P(C_3H_6) = 0.01$ Torr ($N = 3.2 \times 10^{14}$ cm^{-3}), and $P(Ar) = 0.39$ Torr ($N = 1.25 \times 10^{16}$ cm^{-3}) at 298 K. Normalized intensities of consecutive products from the primary ions $[\Sigma(C_6H_6(C_3H_6)_n^{\bullet+})] = [C_6H_6(C_3H_6)^{\bullet+} + C_6H_6(C_3H_6)_2^{\bullet+}]$ and $[\Sigma((C_3H_6)_n^{\bullet+})] = [(C_3H_6)_2^{\bullet+} + (C_3H_6)_3^{\bullet+} + (C_3H_6)_4^{\bullet+} + (C_3H_6)_5^{\bullet+}]$ have been summed to show the distribution into the primary channels.

further reactions. Figure 4 displays the normalized ion intensities of the reactant and product ions of the propene/Ar/benzene system. Evidently the $C_3H_6^{\bullet+}$ monomer ion is formed by charge transfer from Ar^+ and not from $C_6H_6^{\bullet+}$. This is consistent with the endothermicity of 0.48 eV for the charge transfer of $C_6H_6^{\bullet+}$ to propene, which would yield a rate coefficient of $k \leq k_{collision} \exp(-\Delta H^\circ/RT) = 9.7 \times 10^{-18}$ cm^3 s^{-1}, slower by orders of magnitude than the observable limit. On the other hand, the condensation channel leading to the formation of the $(C_3H_6)_n^{\bullet+}$ series with $n = 2-5$ is clearly dominant (80% of all the product ions) as shown in Figure 4. The other major product observed is the $C_6H_6(C_3H_6)_n^{\bullet+}$ series with $n = 1-2$. In addition, the benzene dimer cation $(C_6H_6)_2^{\bullet+}$ is formed and becomes significant at lower concentrations of propene. From the comparison of the data displayed in Figures 3 and 4, it appears that the ionization of the benzene/propene mixture results in the formation of higher propene oligomers $(C_3H_6)_n^{\bullet+}$ and a significant reduction in the product ions typically observed from the bimolecular reactions of $C_3H_6^{\bullet+}$ with C_3H_6 according to reaction 3.

3. R2PI of the Benzene/Propene System. In these experiments, the R2PI of benzene was obtained via the 6^1_0 transition at $\lambda = 258.9$ nm. The two-photon process generates $C_6H_6^{\bullet+}$ ions with excess energy of ≤ 0.32 eV, much lower than the excess energy required for ring opening in ionized benzene, 3.5−5.0 eV.[64] We also note that the two-photon energy of 9.58 eV is lower than the IP of C_3H_6 (9.73 eV).[43] Therefore, the $C_6H_6^{\bullet+}$ ion is generated with small internal energy, and direct charge transfer from an excited $(C_6H_6^{\bullet+})^*$ is also not likely under the HPMS conditions employed in the experiments.

Figure 5 displays the normalized ion intensities following the R2PI of benzene at different concentrations of benzene and propene. At very low concentration of propene, the only product observed is the $C_6H_6^{\bullet+}(C_3H_6)$ adduct. As the concentration of propene increases, the condensation channel $(C_3H_6)_n^{\bullet+}$ starts to open in addition to the adduct channel as shown in Figure 5a, where $(C_3H_6)_n^{\bullet+}$ with $n = 2-4$ and $C_6H_6^{\bullet+}(C_3H_6)_n$ with $n = 1-2$ are the major product channels at benzene and propene number densities of $N(C_6H_6) = 4 \times 10^{12}$ cm^{-3} and $N(C_3H_6) = 5 \times 10^{13}$ cm^{-3}, respectively. As the concentrations of propene increase further, the condensation channel $(C_3H_6)_n^{\bullet+}$ with $n = 2-6$ becomes the major product while the adduct channel $C_6H_6^{\bullet+}(C_3H_6)_n$ with $n = 1-3$ is the minor channel as shown in Figure 5b for $N(C_6H_6) = 9 \times 10^{12}$ cm^{-3} and $N(C_3H_6) = 1 \times 10^{14}$ cm^{-3}. It is also clear that the decay of the benzene ion intensity becomes faster as the concentration of propene increases. Figure 5c shows the normalized ion intensities obtained for the highest concentration of propene used in this study in the absence of Ar ($N(C_3H_6) = 4 \times 10^{16}$ cm^{-3}). In this case, the $(C_3H_6)_n^{\bullet+}$ channel contains up to seven molecules of propene while the $C_6H_6^{\bullet+}(C_3H_6)_n$ channel has $n = 1-3$. It should be noted that the data presented in Figure 5 are used to illustrate the range of the propene additions in both reaction channels under variable concentrations of benzene and propene. For the calculations of the rate coefficient and the product ratio, systematic studies of the effects of propene and Ar concentrations were performed as indicated in Table 1 and discussed in the next section.

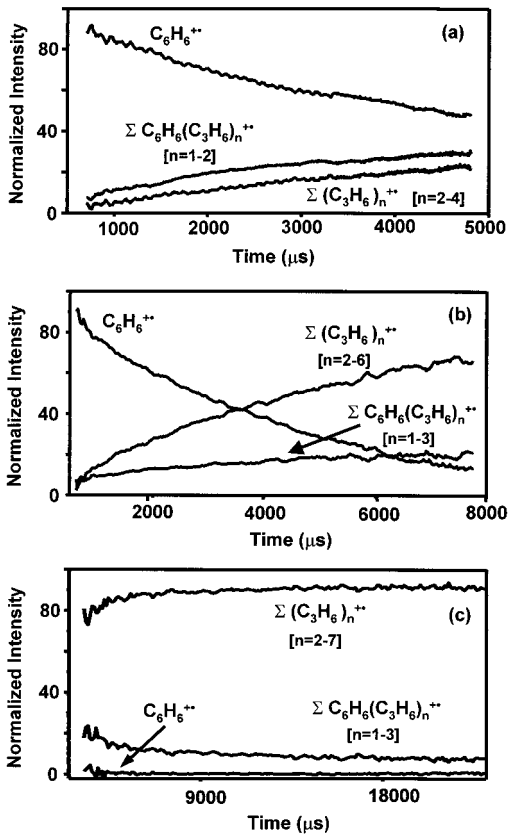

Figure 5. Normalized time profiles in the benzene/propene system at different propene concentrations: (a) $P(C_6H_6) = 0.000\,12$ Torr ($N = 3.72 \times 10^{12}$ cm^{-3}), $P(C_3H_6) = 0.0015$ Torr ($N = 4.89 \times 10^{13}$ cm^{-3}), $P(Ar) = 0.79$ Torr ($N = 2.52 \times 10^{16}$ cm^{-3}); (b) $P(C_6H_6) = 0.000\,29$ Torr ($N = 9.22 \times 10^{12}$ cm^{-3}), $P(C_3H_6) = 0.01$ Torr ($N = 9.9 \times 10^{13}$ cm^{-3}), $P(Ar) = 1.02$ Torr ($N = 3.25 \times 10^{16}$ cm^{-3}); (c) $P(C_6H_6) = 0.000\,32$ Torr ($N = 1.01 \times 10^{13}$ cm^{-3}), $P(C_3H_6) = 1.38$ Torr ($N = 4.42 \times 10^{16}$ cm^{-3}), no argon.

We also observe a secondary product channel corresponding to H_2 transfer from $C_6H_{12}^{\bullet+}$ to form $C_6H_{10}^{\bullet+}$, in analogy with reaction 5, that we observed previously in the toluene$^{\bullet+}$/isobutene system.[38] However, in the benzene$^{\bullet+}$/propene R2PI experiment, $C_6H_{10}^{\bullet+}$ was always a minor product, <7%.

$$C_6H_{12}^{\bullet+} + C_3H_6 \rightarrow C_6H_{10}^{\bullet+} + C_3H_8 \quad (4)$$

$$C_8H_{16}^{\bullet+} + i\text{-}C_4H_8 \rightarrow C_8H_{14}^{\bullet+} + i\text{-}C_4H_{10} \quad (5)$$

TABLE 1: Nominal Second-Order Rate Coefficients for the Reaction[a] of $C_6H_6^{\bullet+}$ with C_3H_6 To Produce $C_6H_{12}^{\bullet+}$ and $C_6H_6(C_3H_6)^{\bullet+}$ [b]

expt no.	[Ar][a]	$[C_3H_6]$[a]	T (K)	k_2[c]	$\Sigma((C_3H_6)_n^{\bullet+})/\Sigma(C_6H_6(C_3H_6)_n^{\bullet+})$[d]	method
1	2.5×10^{16}	1.9×10^{13}	301	2.8	0.4	R2PI−HPMS
2	2.5×10^{16}	3.9×10^{13}	301	2.7	0.8	
3	2.5×10^{16}	9.8×10^{13}	301	2.8	1.8	
4	2.5×10^{16}	1.9×10^{14}	301	3.1	2.1	
5	1.6×10^{16}	4.0×10^{13}	301	2.8	1.0	
6	2.3×10^{16}	4.0×10^{13}	301	3.1	1.0	
7	2.9×10^{16}	4.0×10^{13}	301	3.5	1.0	
8	2.6×10^{16}	1.4×10^{14}	302	2.7[e]	1.6[e]	
9	2.6×10^{16}	1.4×10^{14}	342	1.3[e]	0.7[e]	
10	2.5×10^{16}	8.9×10^{13}	302	2.7	2.8	248 nm MPI
11[f]	1.2×10^{16}[f]		294	1.1[g]	0.4−1.5	SIFT[f]

[a] Number density in molecules cm^{-3}, benzene number density 3.7×10^{12} cm^{-3} in experiments 1−4 and 4.5×10^{12} cm^{-3} in experiments 5−7. [b] Subsequent products in each channel are summed. [c] Units of 10^{-12} cm^3 s^{-1}. Error estimate from replicate measurements ±30%. [d] Product distribution ratio into the primary channels, calculated by summing consecutive higher products in each channel. [e] Average results of two studies, at $[C_3H_6] = 9.9 \times 10^{13}$ (in eq 8) and 1.9×10^{14} (in eq 9) molecules cm^{-3}. [f] In He carrier gas, SIFT experiments. [g] Error estimates $\pm 0.3 \times 10^{-12}$ cm^3 s^{-1}.

4. Reaction Kinetics from the R2PI Experiments. The normalized ion intensities obtained from the R2PI−HPMS experiments are used to calculate rate coefficients as follows. The pseudo-first-order rate coefficient for the overall reaction of $C_6H_6^{\bullet+}$ to products is calculated from the decay of the reactant ion:

$$k_f^1 = -\mathrm{d} \ln [C_6H_6^{\bullet+}]/\mathrm{d}t \quad (6)$$

The corresponding nominal second-order rate coefficient for the overall reaction is calculated using the number density of the reactant $[C_3H_6]$, as

$$k_f^2 = k_f^1/[C_3H_6] \quad (7)$$

The nominal second-order rate coefficients for the two channels are calculated from the product distributions as

$$k_f^2((C_3H_6)_n^{\bullet+}) = k_f^2[\Sigma((C_3H_6)_n^{\bullet+})/(\Sigma((C_3H_6)_n^{\bullet+}) + \Sigma(C_6H_6^{\bullet+}(C_3H_6)_n))] \quad (8)$$

$$k_f^2(C_6H_6^{\bullet+}(C_3H_6)_n) = k_f^2[\Sigma(C_6H_6^{\bullet+}(C_3H_6)_n)/(\Sigma((C_3H_6)_n^{\bullet+}) + \Sigma(C_6H_6^{\bullet+}(C_3H_6)_n))] \quad (9)$$

Rate coefficient measurements were repeated 4−6 times and were reproducible within ±30%. Several measurements were carried out using different concentrations of benzene at fixed propene and Ar concentrations. The overall rate coefficient did not show any dependence on the benzene concentration within the experimental error (±30%).

From the results presented in Table 1, it is clear that the overall coupled charge-transfer/condensation process leading from $C_6H_6^{\bullet+}$ to $C_6H_{12}^{\bullet+}$ proceeds orders of magnitude faster than expected for direct endothermic charge transfer ($\Delta H = +0.48$ eV) from $C_6H_6^{\bullet+}$ to produce the monomer ion $C_3H_6^{\bullet+}$ (observed nominal second-order rate coefficients $k = (1-3) \times 10^{-12}$ cm^3 s^{-1} vs expected $k \leq k_{kollision} \exp(-\Delta H/RT) \approx 10^{-18}$ cm^3 s^{-1}). This is consistent with the fact that the monomer ion $C_3H_6^{\bullet+}$ and its reaction products with C_3H_6 are not observed, and the dimer ion $C_6H_{12}^{\bullet+}$ appears to be formed directly. It is also clear that, at low concentration of propene, the dimer $C_6H_{12}^{\bullet+}$ and the adduct $C_6H_6^{\bullet+}(C_3H_6)$ are formed in parallel, and in comparable yields, as observed clearly in Figure 5a.

The results shown in Table 1 (experiments 1−4) also indicate that the product ratio $\Sigma((C_3H_6)_n^{\bullet+})/\Sigma(C_6H_6^{\bullet+}(C_3H_6)_n)$ increases with increasing propene concentration as expected. However, the product ratio appears to be independent of the carrier gas concentration [Ar] as shown in Table 1 (experiments 5−7). This occurs although the third-body [Ar] that could collisionally stabilize an excited complex to produce $C_6H_6^{\bullet+}(C_3H_6)$ is in excess by factors of 200−1000 over the reactant $[C_3H_6]$ that produces $C_6H_{12}^{\bullet+}$. This is unusual in competitive association/transfer kinetics where the adduct channel usually increases relative to the transfer product with increasing the third-body pressure. Another point of interest can be shown from the limited temperature study of the reaction rate. With increasing temperature, the rate of the reaction into both channels decreases sharply, and the product ratio $\Sigma((C_3H_6)_n^{\bullet+})/\Sigma(C_6H_6^{\bullet+}(C_3H_6)_n)$ decreases as shown in Table 1 (experiments 8 and 9).

5. SIFT Results. In these experiments, the $C_6H_6^{\bullet+}$ ion was generated in a low-pressure ion source by 40 eV electron impact ionization of a 3−5% mixture of C_6H_6 with He. The ions were injected into the flow tube, into which propene was also admitted. The decay of the $C_6H_6^{\bullet+}$ ions showed a fast component and a slow component. The slow component showed chemistry consistent with the R2PI−HPMS observations. The fast component, which was a minor channel (5−7%), showed a different chemistry, suggesting that it may correspond to a $C_6H_6^{\bullet+}$ ion in an isolated electronically excited state formed by the 40 eV electron impact ionization. In fact, the fragment ions $C_3H_3^+$ and $C_4H_4^+$ generated from the benzene ion are known to occur from an excited state that lies ∼2 eV above the ground state of the benzene ion.[65−67]

Figure 6 displays the ion intensities corresponding to the slow reaction component. The lines for $C_6H_6^{\bullet+}$ and $C_6H_6^{\bullet+}(C_3H_6)$ represent a fit of the experimental data with the solution of the system of differential equations for sequential reactions. Other lines are drawn for clarity.

The first step observed is reaction 10, followed by reaction 11, which shows three-way branching.

$$C_6H_6^{\bullet+} + C_3H_6 \rightarrow C_6H_6^{\bullet+}(C_3H_6) \quad (10)$$

$$C_6H_6^{\bullet+}(C_3H_6) + C_3H_6 \rightarrow C_6H_{12}^{\bullet+} + [C_6H_6] \quad (45\%) \quad (11a)$$

$$\rightarrow C_6H_6^{\bullet+}(C_3H_6)_2 \quad (25\%) \quad (11b)$$

$$\rightarrow C_6H_{10}^{\bullet+} + [C_6H_6, H_2] \quad (30\%) \quad (11c)$$

Of the product ions, $(C_3H_6)_6^{\bullet+}$ (not shown in Figure 6) was observed at very high propene flows, formed in a slow reaction

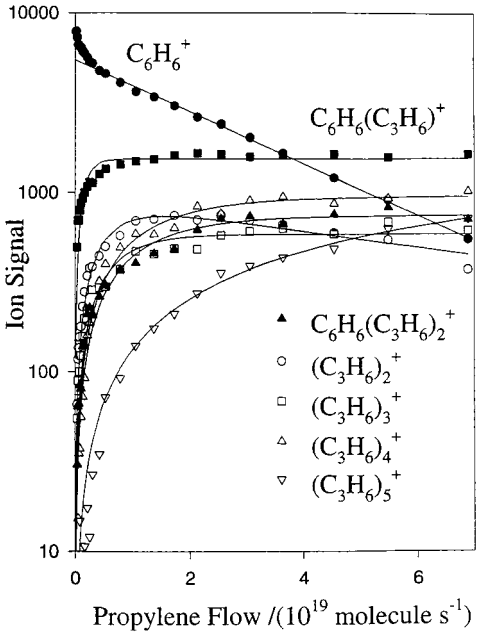

Figure 6. SIFT data for the reaction of $C_6H_6^{\bullet+}$ with C_3H_6 at 294 ± 3 K using He as a buffer gas at a total pressure of 0.35 ± 0.01 Torr. The lines for $C_6H_6^+$ and $(C_6H_6)(C_3H_6)^+$ represent a fit of the experimental data with the solution of differential equations appropriate for the observed sequential reactions. All other lines are drawn for clarity.

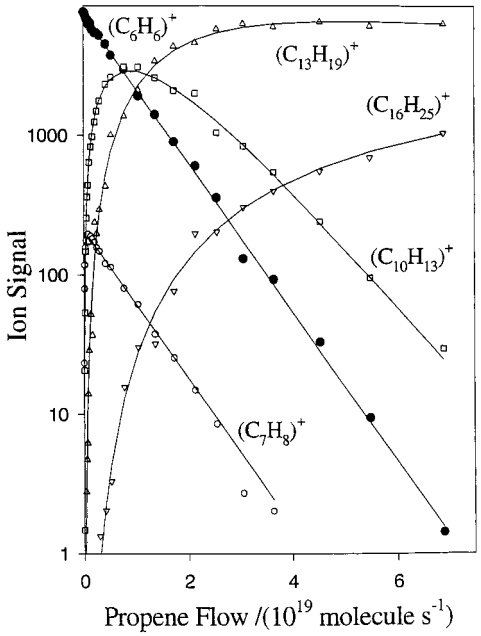

Figure 7. SIFT data for the reaction of $C_6H_6^{\bullet+}$ with C_3H_6 (fast component). The conditions are the same as for the slow part (Figure 6). The slow contributions in high flow parts of the monitored ions were subtracted. The modified experimental data, obtained by this method, were fitted with the solution of differential equations appropriate for the observed sequential reactions.

with a nominal second-order rate coefficient of $k < 5 \times 10^{-14}$ $cm^3\ s^{-1}$.

In the fast decay component, slow reactions contributed only at high propene flows, and the slow reaction contributions were subtracted. The modified experimental plots obtained by this method were fitted with the solution of a system of differential equations for the sequential reactions. The results are shown in Figure 7. The first step (reaction 12) proceeds with a rate coefficient $k = (4.8 \pm 1.3) \times 10^{-12}$ $cm^3\ s^{-1}$ as measured from the fast $C_6H_6^{\bullet+}$ ion decay and the $C_7H_8^{\bullet+}$ product ion increase.

$$C_6H_6^{\bullet+} + C_3H_6 \rightarrow C_7H_8^{\bullet+} + C_2H_4 \qquad (12)$$

The second step (reaction 13) proceeds with a rate coefficient $k = (1.7 \pm 0.5) \times 10^{-10}$ $cm^3\ s^{-1}$.

$$C_7H_8^{\bullet+} + C_3H_6 \rightarrow C_{10}H_{13}^+ + H \qquad (13)$$

Further propene addition steps to form $C_{13}H_{19}^+$ with nominal second-order rate coefficients of $k = (3.9 \pm 1.5) \times 10^{-12}$ $cm^3\ s^{-1}$ and subsequently $C_{16}H_{25}^+$ with $k = (1.2 \pm 0.8) \times 10^{-12}$ $cm^3\ s^{-1}$ and $C_{19}H_{31}^+$ with $k < 5 \times 10^{-14}$ $cm^3\ s^{-1}$ were observed at high propene flows according to reactions 14 and 15.

$$C_{10}H_{13}^+ + C_3H_6 \rightarrow C_{13}H_{19}^+ \qquad (14)$$

$$C_{13}H_{19}^+ + C_3H_6 \rightarrow C_{16}H_{25}^+ \qquad (15)$$

The different chemistry of this $C_6H_6^{\bullet+}$ component suggests that it may be an excited ion formed in the 40 eV ionization.

6. Reaction Mechanism. The kinetic trends observed in the current system are similar to those observed in the toluene$^{\bullet+}$/isobutene system, and they suggest a similar mechanism.[38] First, direct charge transfer from $C_6H_6^{\bullet+}$ to C_3H_6 can be ruled out on the basis of the results discussed above. Another possible mechanism would be analogous to other ion/molecule competitive transfer/association reactions as outlined in Scheme 1.

SCHEME 1

$$C_6H_6^{\bullet+} + C_3H_6 \rightleftarrows [C_6H_6^{\bullet+}(C_3H_6)]^* \xrightarrow{C_3H_6} C_6H_{12}^{\bullet+} + C_6H_6$$

$$\xrightarrow{Ar} C_6H_6^{\bullet+}(C_3H_6)$$

The stabilization efficiency of a relatively large atomic species such as Ar is expected to be 0.1−1. Accordingly, for example in the first experiment in Table 1, the $\Sigma((C_3H_6)_n^{\bullet+})/\Sigma(C_6H_6^{\bullet+}(C_3H_6)_n)$ product ratio should be in the range 0.001−0.01. The actual observed ratio is larger by a factor of 40−400 than expected and is independent of [Ar] (experiments 5−7 in Table 1). These results are not consistent with Scheme 1. We therefore suggest the mechanism shown in Scheme 2.

SCHEME 2

$$C_6H_6^{\bullet+} + C_3H_6 \rightleftarrows [C_6H_6^{\bullet+}(C_3H_6)]^* \overset{Ar}{\rightleftharpoons}$$

$$[C_6H_6^{\bullet+}(C_3H_6)] \xrightarrow{C_3H_6} C_6H_{12}^{\bullet+} + C_6H_6$$

$$\rightarrow C_6H_5C_3H_7^{\bullet+}$$

Here the excited complex $[C_6H_6^{\bullet+}(C_3H_6)]^*$ is first stabilized collisionally to the thermalized π complex $C_6H_6^{\bullet+}(C_3H_6)$ stabilized by ion-induced dipole forces. This complex reacts further with C_3H_6, in competition with unimolecular rearrangement to a probably covalently bonded adduct, propylbenzene cation $C_6H_5C_3H_7^{\bullet+}$. This is known to occur in several similar systems such as benzene$^{\bullet+}$/butadiene and (styrene)$_2^{\bullet+}$.[68−72] The rearrangement is pseudo-first-order, possibly at high-pressure limiting kinetics. It is easy to see that, qualitatively, the mechanism justifies all of the observations discussed above. Specifically, the product ratio $\Sigma((C_3H_6)_n^{\bullet+})/\Sigma(C_6H_6^{\bullet+}(C_3H_6)_n)$ is independent of [Ar] but increases with [C_3H_6] as observed.

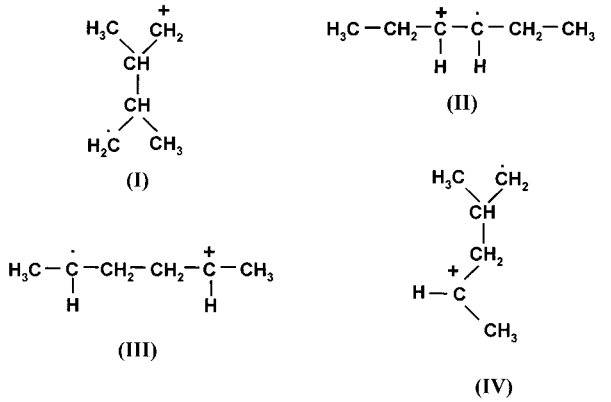

Figure 8. Possible structures of the $C_6H_{12}^{\bullet+}$ ion.

Significantly, the overall rate coefficients obtained from the decay of the benzene ion for similar reaction compositions and source pressures in both the R2PI and the 248 nm MPI experiments are remarkably consistent (experiments 3 and 10 in Table 1). Therefore, the small concentration of $C_3H_6^{\bullet+}$ produced from nonresonance ionization had no significant effect on the coupled reactions involved in the overall process (2).

Within the limited pressure range available, the overall rate coefficient seems to increase with [Ar] as expected (Table 1, experiments 5−7). However, we note that the rate coefficient measurements are relatively inaccurate in the present system, because of the slow kinetics. In the faster and more accurately measured toluene/isobutene system, the rate coefficient showed the expected pressure dependence.[38] We also note here that comparing the rate coefficient measured in the R2PI−HPMS vs the SIFT measurement at lower pressure and with the less efficient, He third body shows the expected trend.

The temperature dependence of the product distribution ratio shows that the $\Sigma((C_3H_6)_n^{\bullet+})/\Sigma(C_6H_6^{\bullet+}(C_3H_6))$ ratio increases at lower temperatures. This can be explained by larger activation energy for the unimolecular rearrangement of $[C_6H_6^{\bullet+}(C_3H_6)]$ to $C_6H_5C_3H_7^{\bullet+}$, while its exothermic bimolecular reaction with C_3H_6 to give $C_6H_{12}^{\bullet+}$ may have a smaller, or negligible, activation energy.

Although the two-point temperature study in Table 1 cannot define the functional form of temperature coefficients, the temperature dependence of several types of ion/molecule reactions is of the form $k = aT^{-n}$. Calculation of the partial rate coefficients for the two channels (eqs 8 and 9) leads to the temperature coefficients of the nominal second-order rate coefficients $k[(C_3H_6)_2^{\bullet+}] = aT^{-9.0}$ and $k[C_6H_6^{\bullet+}(C_3H_6)] = aT^{-2.4}$. Extrapolating from the 302 K values, $k[(C_3H_6)_2^{\bullet+}]$ and $k[C_6H_6^{\bullet+}(C_3H_6)]$ will reach the collision rate of 10^{-9} cm^3 s^{-1} at 148 and 18 K, respectively. These trends suggest that reaction 2 and, in general, Scheme 2 may lead to efficient reactions at low planetary atmospheric and interstellar temperatures. For example, ionized aromatics are assumed to be present in interstellar environments.[73,74] Several polymerizable molecules can accumulate on the ionized molecular surface until a coupled charge-transfer/polymerization process becomes energetically possible. The reaction may involve more than two monomer molecules. For example, we made spectroscopic observations in the *p*-xylene$^{\bullet+}$/isobutene system which suggested isobutene dimer formation with the participation of several isobutene molecules in a cluster.[30,38]

7. Structures of the Product Ions. Four possible structures of $C_6H_{12}^{\bullet+}$ are shown in Figure 8. Structures **I** and **II** are proposed by Abramson and Futrell.[48,49] A different linear form (**III**) of a distonic type based on the structure of 3-hexene is suggested by Peers.[50] The important feature of structure **III** distinguishing it from structure **II** is that there is no net H-atom shift if C_2H_4 is to be eliminated. In addition, the formation of $C_4H_8^{\bullet+}$ requires breaking only one C−C bond, compared to structure **I** which would require breaking two C−C bonds for the loss of C_2H_4. However, for the loss of an ethyl radical, $C_2H_5^{\bullet}$, structure **II** is more favorable than **III**. Structure **IV** is suggested by Henis[51] on the basis of the criteria that no significant rearrangement of the parent ions occurs in the complex formation, addition occurs at either end of the double bond, and fragmentation involving more than one bond is not favorable.

In the present MPI−HPMS experiment involving propene/Ar mixtures in the absence of benzene, the $C_4H_8^{\bullet+}$ ions have no significant yield while the observed intensity of $C_4H_7^+$ is about 48% of the total ion yield as shown in Figure 3. Therefore, structure **II** appears to be more consistent with our data.

We note that, in the benzene/propene experiments, the IP of the C_6H_{12} molecule corresponding to the product ion $C_6H_{12}^{\bullet+}$ must be <9.25 eV; otherwise the reaction complex would dissociate to yield $C_6H_6^{\bullet+}$ primarily. This rules out cyclic $C_6H_{12}^{\bullet+}$, as the IP of c-C_6H_{12} is 9.86 eV.[43] Also, on the basis of the work of Ausloos et al., the cyclic $C_6H_{12}^{\bullet+}$ could undergo a H_2-transfer reaction with C_3H_6 to produce a cyclic ion, $C_6H_{10}^{\bullet+}$, and C_3H_8.[52,53] In fact, only minor product $C_6H_{10}^{\bullet+}$ ions (7%) were observed in this R2PI−HPMS experiment contrary to the SIFT experiment, where the $C_6H_{10}^{\bullet+}$ ions constitute about 30% of the product ions. Therefore, it is expected that the majority of the $C_6H_{12}^{\bullet+}$ ions produced in both the HPMS and SIFT experiments may have a linear structure, although a cyclic form may also be present under the conditions of the SIFT experiment. Energetically, the most favored product is the most stable $C_6H_{12}^{\bullet+}$ isomer, which corresponds to the neutral molecule $(CH_3)_2C{=}C(CH_3)_2$ with the lowest ΔH^o_f of 174 kcal/mol.[75] With this product, reaction 2 is exothermic by 48.7 kcal/mol. This product can form with only hydrogen shifts from the reactants, without requiring skeletal rearrangement.

The observation of higher order additions on the $C_6H_{12}^{\bullet+}$ dimer in the benzene/propene experiments, including up to seven molecules of propene with no pronounced magic number, suggests that no cyclization takes place during the growth of the $(C_3H_6)_n$ ions. This result is different from the observation of intracluster polymerization reactions, where magic numbers are often observed and interpreted as due to the formation of cyclic stable ions.[13,30,37]

8. Benzene/Propene Binary Clusters. Figure 9 displays the mass spectrum obtained by the R2PI (λ = 259.60 nm) of benzene/propene clusters generated by supersonic expansion. Note that the absorption of the mixed clusters is red-shifted from the 6_0^1 resonance of benzene at 258.90 nm. This is expected on the basis of the predominant dispersion force interaction between benzene and propene, which leads to the observed red shift in the 6_0^1 transition of benzene.

At 259.60 nm, the sum of the two-photon energies is 9.57 eV, which is less than the IP of propene, 9.73 eV, as we noted above. Consequently, no $C_3H_6^{\bullet+}$ is observed in the mass spectrum and only higher clusters of $(C_3H_6)_n^{\bullet+}$ with $n \geq 2$ are produced by the R2PI. Similar results were obtained by nonresonant MPI using the 248 and 193 nm photons. At lower laser fluency, the power dependence of the $C_6H_6^{\bullet+}$ ion intensity indicates that the ions are formed via a two-photon absorption process.

An interesting feature in the benzene/propene clusters is the observation of a magic number within the $(C_3H_6)_n^{\bullet+}$ series

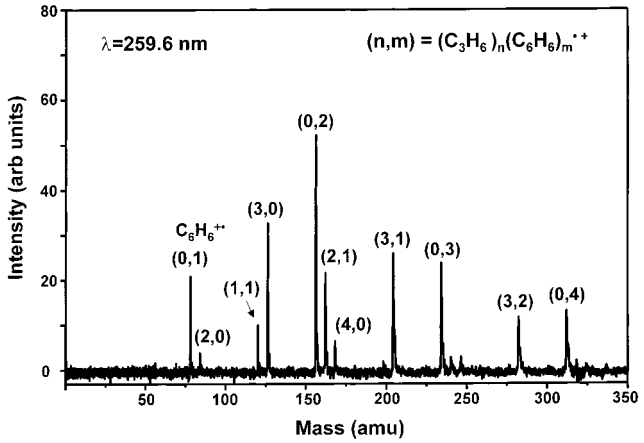

Figure 9. Mass spectrum of propene/benzene mixed clusters $(C_3H_6)_n(C_6H_6)_m$ taken at 259.60 nm. Preexpansion mixture: 16.5% propene and 0.0083% benzene in helium at a total pressure of 1300 Torr.

corresponding to $n = 3$. This feature also persists in the presence of benzene molecules in the cluster, and therefore, the same magic number for $n = 3$ is observed in the mixed clusters $(C_3H_6)_n(C_6H_6)_m$ for all the values of m observed under our experimental conditions (up to $m = 10$). A similar result was reported for the electron impact ionization of neat propene clusters and was attributed to the formation of a cyclic $(C_3H_6)_3^{\bullet+}$, which can serve as an energy trap by making further reactions energetically unfavorable.[13,37] This energy trap would be effective in low-temperature clusters formed by the evaporation of monomers. Similar behavior has been observed in the EI ionization of isobutene clusters under low EI energies.[30] The observation of enhanced intensity for the trimer ion $(C_4H_8)_3^{\bullet+}$ has been explained in terms of cyclization of the radical cation $C_{12}H_{24}^{\bullet+}$ to form a stable and less reactive isomer, which can interrupt the pattern of successive addition reactions.

The observation of the magic number $n = 3$ within the mixed clusters $(C_3H_6)_n(C_6H_6)_m$ suggests that the cyclic $(C_3H_6)_3^{\bullet+}$ interacts favorably with the benzene molecules. This may be due to structural similarity, which makes $(C_3H_6)_3^{\bullet+}$ an efficient substitute for $C_6H_6^{\bullet+}$ in the $(C_6H_6)_m^{\bullet+}$ cluster series. The magic number feature also implies that $(C_3H_6)_3^{\bullet+}$ is the core ion within the $(C_6H_6)_m(C_3H_6)_n^{\bullet+}$ series, which indicates that the cyclic $(C_3H_6)_3$ has an IP lower than that of benzene clusters and, therefore, the charge resides on the $(C_3H_6)_3$ moiety. It is important to point out that the observation of a magic number corresponding to the formation of a cyclic propene trimer within the clusters is different from the gas-phase results, where higher propene oligomers were observed with no evidence of the formation of stable cyclic structures which could interrupt the sequential addition reactions. This difference may be attributed to the different efficiencies of cluster evaporation and gas-phase collisional stabilization. In addition, the lower temperature of the cluster ions (~80 K) as compared to the gas phase could result in different isomeric forms of the propene oligomers. It is expected that, under the low-temperature cluster condition, cyclization of the radical cations may take place and, therefore, gives rise to the observation of the magic numbers.

IV. Summary and Implications for Polymerization

In this paper, we presented a detailed study of the coupled reactions between ionized benzene and propene molecules in the gas phase and in preformed benzene/propene clusters. The gas-phase results obtained by high-pressure mass spectrometry using R2PI and MPI techniques are consistent with the SIFT results, where benzene cations formed by EI are injected into a flow tube containing a propene/He gas mixture. The gas-phase results are also consistent with the reactions observed following the R2PI of the clusters. In all of these studies, the main observation is coupled reactions of dimer formation and charge transfer followed by sequential reactions to produce propene oligomer ions $(C_3H_6)_n^{\bullet+}$ with $n = 2-7$. The observed kinetic trends in the gas phase, especially the pressure effects, are best reproduced by a mechanism through a collisionally stabilized noncovalent intermediate complex, $C_6H_6^{\bullet+}(C_3H_6)$, in which the propene molecule is "adsorbed" on the ionized benzene surface, and assumes a charge density by interaction with the aromatic ion. Upon collision with another propene molecule, in the resulting $C_6H_6^{\bullet+}(2C_3H_6)$ complex, one olefin molecule can carry sufficient charge density to activate it for nucleophilic attack by the second propene molecule, resulting in covalent condensation. Formation of a hexene molecule with a lower IP than benzene will then result in full charge transfer, leading to the observed product ion.

The present mechanism avoids the formation of the olefin monomer ions and their reaction products, suggesting a useful photoinitiation method for pure products. In the present system we observed the exclusive formation of $(propene)_n^{\bullet+}$ with $n = 2-7$. In contrast, ion/molecule reactions between $C_3H_6^{\bullet+}$ and C_3H_6 produce $C_3H_7^+$, $C_4H_7^+$, $C_4H_8^{\bullet+}$, and $C_5H_9^+$ that can further polymerize.[44−59] We noted the similarity of the reaction mechanism in the gas phase and in preformed clusters.[29,30,32,38] It would be interesting to explore the application of this mechanism in the condensed phase using common aromatic solvents such as benzene and toluene. The solvent photoinitiation mechanism may lead to a "*solvent as initiator approach*" to eliminate chemical initiators, with beneficial economic and environmental results.

Acknowledgment. This research is supported by the National Science Foundation (Grant CHE 9816536). Acknowledgment is also made to the NASA Microgravity Materials Science Program (Grant NAG8-1484) for the partial support of this research. D.K. Bohme acknowledges support from the Natural Sciences and Engineering Research Council of Canada.

References and Notes

(1) Pithawalla, Y. B.; El-Shall, M. S. In *Solvent-Free Polymerizations and Processes: Minimization of Conventional Organic Solvents*; Long, T. E., Hunt, M. O., Eds.; ACS Symposium Series 713; American Chemical Society: Washington, DC, 1998; pp 232−247.
(2) Pool, R. *Science* **1990,** *248*, 1186.
(3) Perrin, J.; Despax, B.; Hanchett, V.; Kay, E. *J. Vac. Sci. Technol., A* **1986**, *4*, 46.
(4) Kay, E. *Z. Phys. D* **1986**, *3*, 251.
(5) El-Shall, M. S.; Slack, W. *Macromolecules* **1995**, *28*, 8546.
(6) El-Shall, M. S. *Appl. Surf. Sci.* **1996**, *106*, 347.
(7) Raksit, A. B.; Bohme, D. K. *Can. J. Chem.* **1984**, *62*, 2123.
(8) Forte, L.; M. H. Lien, M. H.; Hopkinson, A. C.; Bohme, D. K. *Makromol. Chem., Rapid Commun.* **1987**, *8*, 87.
(9) Forte, L.; Lien, M. H.; Hopkinson, A. C.; Bohme, D. K. *Can. J. Chem.* **1989**, *67*, 1576.
(10) El-Shall, M. S.; Marks, C. *J. Phys. Chem.* **1991**, *95*, 4932.
(11) El-Shall, M. S.; Schriver, K. E. *J. Chem. Phys.* **1991**, *95*, 3001.
(12) Tsukuda, T.; Kondow, T. *J. Chem. Phys.* **1991**, *95*, 6989.
(13) Coolbaugh, M. T.; Vaidyanathan, G.; Peifer, W. R.; Garvey, J. F. *J. Phys. Chem.* **1991**, *95*, 8337.
(14) Wang, J.; Javahery, G.; Petrie, S.; Bohme, D. K. *J. Am. Chem. Soc.* **1992**, *114*, 9665.
(15) Tsukuda, T.; Kondow, T. *J. Phys. Chem.* **1992**, *96*, 5671−5673.
(16) Tsukuda, T.; Kondow, T. *Chem. Phys. Lett.* **1992**, *197*, 438.
(17) Tsukuda, T.; Terasuki, A.; Kondow, T.; Scarton, M. G.; Dessent, C. E.; Bishea, G. A.; Johnson, M. A. *Chem. Phys. Lett.* **1993**, *201*, 351.
(18) Guo, B. C.; Castleman, A. W., Jr. *J. Am. Chem. Soc.* **1992**, *114*, 6152.
(19) Daly, G. M.; El-Shall, M. S. *Z. Phys. D* **1993**, *26s*, 186.

(20) Vann, W.; El-Shall, M. S. *J. Am. Chem. Soc.* **1993**, *115*, 4385.
(21) Vann, W.; Daly, G. M.; El-Shall, M. S. *Mater. Res. Soc. Symp. Proc. Ser.* **1993**, *285*, 593.
(22) Brodbelt, J. S.; Liou, C. C.; Maleknia, S.; Lin, T. J.; Lagow, R. J. *J. Am. Chem. Soc.* **1993**, *115*, 11069.
(23) Daly, G. M.; El-Shall, M. S. *J. Phys. Chem.* **1994**, *98*, 696.
(24) Wang, J.; Javahery, G.; Petrie, S.; Hopkinson, A. C.; Bohme, D. K. *Angew. Chem., Int. Ed. Engl.* **1994**, *33*, 206.
(25) Tsukuda, T.; Kondow, T. *J. Am. Chem. Soc.* **1994**, *116*, 9555.
(26) Desai, S. R., Feigerle, C. S., Miller, J. *J. Phys. Chem.* **1995**, *99*, 1786.
(27) Daly, G. M.; El-Shall, M. S. *J. Phys. Chem.* **1995**, *99*, 5283.
(28) Daly, G. M.; Pithawalla, Y. B.; Yu, Z.; El-Shall, M. S. *Chem. Phys. Lett.* **1995**, *237*, 97.
(29) Meot-Ner (Mautner), M.; Sieck, L. W.; El-Shall, M. S.; Daly, G. M. *J. Am. Chem. Soc.* **1995**, *117*, 7737.
(30) El-Shall, M. S.; Daly, G. M.; Yu, Z.; Meot-Ner (Mautner), M. *J. Am. Chem. Soc.* **1995**, *117*, 7744.
(31) Baranov, V.; Wang, J.; Javahery, G.; Hopkinson, A. C.; Bohme, D. K. *J. Am. Chem. Soc.* **1997**, *119*, 2040.
(32) El-Shall, M. S.; Yu, Z. *J. Am. Chem. Soc.* **1996**, *117*, 13058.
(33) Pithawalla, Y. B.; J. Gao, J.; Yu, Z.; El-Shall, M. S. *Macromolecules* **1996**, *29*, 8558.
(34) Bjarnason, A.; Ridge, D. P. *J. Phys. Chem.* **1996**, *100*, 15118.
(35) Tsukuda, T.; Kondow, T.; Dessent, C. E. H.; Bailey, C. C.; Johnson, M. A.; Hendricks, J. H.; Lyapustina, S. A.; K. H. Bowen, K. H. *Chem. Phys. Lett.* **1997**, *269*, 17.
(36) Morita, H.; Freitas, J. E.; El-Sayed, M. A. *J. Phys. Chem.* **1997**, *101*, 3699.
(37) Zhong, Q.; Poth, L.; Shi, Z.; Ford, J. V.; Castleman, A. W., Jr. *J. Phys. Chem.* **1997**, *101*, 4203.
(38) Meot-Ner (Mautner), M.; Pithawalla, Y. B.; Gao, J.; El-Shall, M. S. *J. Am. Chem. Soc.* **1997**, *119*, 8332.
(39) Christ, C. S.; Eyler, J. R.; Richardson, D. E. *J. Am. Chem. Soc.* **1988**, *110*, 4038; **1990**, *112*, 596.
(40) Alameddin, N. G.; Ryan, M. F.; Eyler, J. R.; Siedle, A. R.; Richardson, D. E. *Organometallics* **1995**, *14*, 5006.
(41) Reference deleted on revision.
(42) Feichtinger, D.; Plattner, D. A.; Chen, P. *J. Am. Chem. Soc.* **1998**, *120*, 7125.
(43) Levin, R. D.; Lias, S. G. *Ionization Potential and Appearance Potential Measurements, 1971−1981*; National Bureau of Standards: Washington, DC, 1982.
(44) Harrison, A. G. *Can. J. Chem.* **1962**, *41*, 236.
(45) Koyano, I.; Omura, I.; Tanaka, I. *J. Chem. Phys.* **1966**, *44*, 3850.
(46) Aquilanti, V.; Galli, A.; Giardin-Guidoni; Vopli, G. G. *Trans. Faraday Soc.* **1967**, *63*, 926.
(47) Sieck, L. W.; Futrell, J. H. *J. Chem. Phys.* **1966**, *45*, 560.
(48) Abramson, F. P.; Futrell, J. H. *J. Phys. Chem.* **1968**, *72*, 1994.
(49) Abramson, F. P.; Futrell, J. H. *J. Phys. Chem.* **1968**, *72*, 1826.
(50) Peers, A. M. *J. Phys. Chem.* **1969**, *73*, 4141.
(51) Henis, J. M. S. *J. Chem. Phys.* **1970**, *52*, 282.
(52) Gorden, R., Jr.; Doepker, R.; Ausloos, P. *J. Chem. Phys.* **1966**, *44*, 3733.
(53) Ausloos, P.; Lias, S. G. *J. Chem. Phys.* **1965**, *43*, 127.
(54) Herod, A. A.; Harrison, A. G. *J. Phys. Chem.* **1969**, *73*, 3189.
(55) Herod, A. A.; Harrison, A. G.; O'Malley, R. M.; Ferrer-Correia, A. J.; Jennings, K. R. *J. Phys. Chem.* **1970**, *74*, 2583.
(56) Bowers, M. T.; Elleman, D. D.; O'Malley. R. M.; Jennings, K. R. *J. Phys. Chem.* **1970**, *74*, 2583.
(57) Bowers, M. T.; Aue, D. H.; Elleman, D. D. *J. Am. Chem. Soc.* **1972**, *94*, 4255.
(58) Sieck, L. W.; Searles, S. K. *J. Am. Chem. Soc.* **1970**, *92*, 2937.
(59) Tzeng, W. B.; Ono, Y.; Linn, S. H.; Ng, C. Y. *J. Chem. Phys.* **1985**, *83*, 2803.
(60) Daly, G. M.; Meot-Ner (Mautner), M.; Pithawalla, Y. B.; El-Shall, M. S. *J. Chem. Phys.* **1996**, *104*, 7965.
(61) Mackay, I.; Vlachos, G. D.; Bohme, D. K.; Schiff, H. I. *Int. J. Mass Spectrom. Ion Phys.* **1980**, *36*, 259. Raksit, A. B.; Bohme, D. K. *Int. J. Mass Spectrom. Ion Processes* **1984**, *55*, 69.
(62) Baranov, V.; Wang, J.; Javahery, G.; Hopkinson, A. C.; Bohme, D. K. *J. Am. Chem. Soc.* **1997**, *119*, 2040.
(63) Wiley: W. C.; McLaren, I. *Rev. Sci. Instrum.* **1955**, *26*, 1150.
(64) Bosel, U.; Neusser, H. J.; Schlag, E. W. *J. Chem. Phys.* **1980**, *72*, 4327.
(65) Rosenstock, H. M.; Larkins, J. T.; Walker, J. A. *Int. J. Mass Spectrom. Ion Phys.* **1973**, *11*, 309.
(66) Rosenstock, H. M.; McColloh, K. E.; Lossing, F. P. *Int. J. Mass Spectrom. Ion Phys.* **1977**, *25*, 327.
(67) Eland, J. H. D. *Int. J. Mass Spectrom.* **1974**, *62*, 3835.
(68) Groenewold, G. S.; Chess, E. K.; Gross, M. L. *J. Am. Chem. Soc.* **1984**, *106*, 539.
(69) Chess, E. K.; Lin. P. H.; Gross, M. L. *J. Org. Chem.* **1983**, *48*, 1522.
(70) Russell, D. H.; Gross, M. L. *J. Am. Chem. Soc.* **1980**, *102*, 6279.
(71) Groenewold, G. S.; Gross, M. *J. Am. Chem. Soc.* **1984**, *106*, 6575.
(72) Holman, R. W.; Rozeboom, M. D.; Gross, M. L.; Warner, C. D. *Tetrahedron* **1986**, *42*, 6235.
(73) Dalgarno, A. *J. Chem. Soc., Faraday Trans.* **1993**, *89*, 2111.
(74) Bohme, D. K. *Chem. Rev.* **1992**, *92*, 1487. Petrie, S.; Bohme, D. K. *Astrophys. J.* **1994**, *436*, 411.
(75) Lias, S. G.; Liebman, J. F.; Levin, R. D.; Kafafi, S. A.; Stein, S. E. NIST Standard Reference Database 19A, Version 2.01, January 1994.